FLIGHT EVIDENCE OF SPACECRAFT SURFACE CONTAMINATION RATE ENHANCEMENT BY SPACECRAFT CHARGING OBTAINED WITH A QUARTZ CRYSTAL MICROBALANCE*

D. M. Clark and David F. Hall
The Aerospace Corporation

SUMMARY

A goal of the ML-12 experiment is to determine whether a significant fraction of the mass outgassed by a negatively charged space vehicle is ionized within the vehicle plasma sheath and electrostatically reattracted to the space vehicle. The ML-12 retarding potential analyzer/temperature controlled quartz crystal microbalances (RPA/TQCMs) were designed to distinguish between charged and neutral molecules in order to investigate this contamination mass transport mechanism. In this paper, a preliminary analysis is given of two long-term, quick-look flight data sets, which indicates that on average a significant fraction of mass arriving at one RPA/TQCM was ionized. (Data from the other instrument have been difficult to analyze.) An important assumption is made in the analysis: that vehicle frame charging during these periods was approximately uniformly distributed in degree and frequency. The data are generally consistent with this asumption. These experiments provide evidence that electrostatic reattraction of ionized molecules is an important contamination mechanism at and near geosynchronous altitudes. Some implications of this conclusion for space vehicle design are discussed.

INTRODUCTION

It has been proposed that spacecraft charging increases the rate of deposition of contamination on spacecraft surfaces (ref. 1). A major objective of the ML-12 experiment is to determine whether this increase in contamination rate is large enough to significantly shorten the useful life of critical spacecraft subsystems (ref. 2). The proposed mass transport mechanism and the placement of the ML-12 experiment sensors on the P78-2 spacecraft are illustrated in figure 1. The idea is that some of the molecules released from the spacecraft by outgassing, electrical discharges, and thruster operations are ionized by energetic photons or energetic electrons before they reach the boundary of the plasma sheath that surrounds the vehicle when it is negatively charged. Because these ions are positively charged, they would be electrostatically reattracted to the vehicle.

* Work supported by the U.S. Air Force, AFWAL/MLBE WPAFB, and SD, LAAFS, under contract F04701-80-C-0081.

Theoretical estimates of the fraction of released molecules that would be returned by this mechanism vary considerably and require severely simplifying assumptions.

The instrument designed to investigate this phenomenon is a combination of a retarding potential analyzer (RPA) and temperature controlled quartz crystal microbalance (TQCM), as shown in figure 2. Details of this instrument are given in references 2 through 4. Note that the charged particle collector is annular, so that some of the incoming particles reach it and some reach the mass sensor. The potential diagram in figure 3 illustrates the spacecraft frame $V_{s/c}$ at -100 V with respect to the ambient plasma potential. Three cases of positive RPA grid bias are also shown. A slow molecule ionized at point D could reach the mass or charge collector if the grid were biased as in cases C and B, but not in case A.

Eight different settings of the retarding potential analyzer grid voltage (RPAV) can be commanded: -100, -10, -1, 0, 1, 10, 100, and 500 V. Whenever the vehicle frame potential is less negative than the grid is positive ($|V_{s/c}| < RPAV$), all the ionized contamination molecules will be reflected. Then only uncharged mass will be collected on the TQCM sensing surface, the potential of which is also $V_{s/c}$. Conversely, when the vehicle frame is more negative than the grid is positive ($|V_{s/c}| > RPAV$), molecules ionized close to the vehicle will be reflected by the grid, whereas those ionized further away but still within the vehicle sheath can be collected. When $RPAV < 0$, ion collection is unaffected, but electron collection is affected.

These ideas are summarized in figure 4, which reveals a qualitative indication of the expected dependence of mass accumulation rate ($\dot{M}$) on RPAV for a case where $-100 > V_{s/c} > -500$. When RPAV is 500 V, only un-ionized molecules are measured ($\dot{M} = \dot{M}^{o}$); when $RPAV < 0$, all ionized molecules with appropriate trajectories are also collected ($\dot{M} = \dot{M}^{o} + \dot{M}^{+}$). In theory, determination of the importance of spacecraft charging on contamination rate, i.e., determination of $\dot{M}^{+}/\dot{M}^{o}$, is straightforward with this instrument; in practice, it is difficult for the following reasons.

The P78-2 is a relatively clean vehicle with an outgassing rate that is probably significantly less than that of many spacecraft. This results in values of $\dot{M}$ that must be integrated over hours, if not days, in order to be reliably determined.

The P78-2 also charges to large potentials very infrequently, and then only for relatively short periods of time. (The larger $V_{s/c}$ is, the greater is the extent of the sheath and the higher the probability of molecular ionization within it.) According to studies conducted by C.K. Purvis with NASA Charging Analyzer Program (NASCAP) (ref. 5), the P78-2 configuration is not as favorable to charging as are configurations typical of three-axis stabilized vehicles. The largest charging events identified have been less than 1 hour in duration and have taken place during eclipses. Enhancement of

$\dot{M}$ has not been detected during these events because thermal effects on the ML12-6 and -7 mass sensors increased detection thresholds by factors of 80 and 4, respectively, and because the main mechanism of molecular ionization, photoionization, is absent during eclipses.

Reliable determination of $V_{s/c}$ when $0 > V_{s/c} > -100$ V is sometimes difficult. Because of photoemission from vehicle surfaces, noneclipse charging is usually in this range.

Capabilities to predict or detect spacecraft charging events are meager at present. In fact, it is generally not known until months later whether a moderate event has taken place, because spectrometer data, from which spacecraft charging events are most reliably detected, are generally not available for at least 6 months after the data are collected. Therefore, with the exception of operations during artificial charging events produced by the SC4-2 ion gun, spacecraft charging experiments cannot be planned in advance.

In this paper are reported two experiments that deal with these difficulties statistically. The assumptions made are: (1) charging events are approximately uniformly distributed in time, (2) charging events are large enough, long enough, and frequent enough to make $\dot{M}^+/\dot{M}^o$ detectable, (3) the rate and composition of mass release from the vehicle are approximately constant over an experimental period, and (4) the adsorption characteristics of mass incident on the mass detector are constant with time. In both experiments, the aperture grid was connected to the spacecraft frame, as shown in figure 2. The coating over the mirrors surrounding the aperture and the skin of the spacecraft out to 25 cm from the aperture are electrically conductive and are also connected to the space vehicle frame. Therefore the electric field in the vicinity of the aperture must be relatively uniform and perpendicular to the aperture plane. The RPA grid voltage was commanded to selected values for periods of 10 or more days, and $\dot{M}$ values averaged over 5-day segments were compared.

In the first (winter) experiment, a greater than 90 percent confidence was obtained that $\dot{M}$ is negatively correlated with RPAV, i.e., that some incoming mass is reflected by the grid when it is positively biased. This fraction of the mass must have been positively ionized. The outcome of the recently concluded second (summer) experiment is not as easily assessed. The validity of data from three of the eight experiment segments is questionable and not as yet resolved. Some evidence of negative correlation is obtained when these data points are included in experiment analysis. If the questionable data points are excluded from the summer analysis, however, there is strong evidence of the negative correlation of $\dot{M}$ with RPAV.

EXPERIMENTAL OBSERVATIONS

Analysis of data from these experiments has been complicated by several extraneous effects that affect the TQCM data. These effects are discussed separately for ML12-6 and ML12-7.

Extraneous ML12-6 Effects

The average ML12-6 TQCM mass accumulation rate has always been significantly greater than that of the ML12-7, except during an unusual period in July and August 1980. This has been ascribed to the fact that ML12-6 receives sunlight while ML12-7 is shadowed (ref. 6). This photochemical effect is "extraneous" because it tends to mask the effect of electrostatic reattraction of ions, but it is not an "instrumental" effect. Two other facets of this effect are discussed here.

The first new observation is that the value of $\dot{M}_6$ is affected by boom shadowing. This was noticed from study of long-term ML12-6 mass accumulation versus time plots. In general, the time derivative of these plots ($\dot{M}_6$) has minima occurring a few days prior to each maneuver (figure 5). Further investigation of M_6 data and vehicle attitude information disclosed a direct relationship between vehicle sun angle (SANG), observed ML12-6 TQCM sensor temperature (T_6), and M_6, as shown in figure 6. These relationships are generally consistent with the predictions made with a NASCAP routine of ML12-6 shadowing by booms, as summarized in table I (ref. 7). Thus, $\dot{M}_6$ is diminished during periods of shadowing compared with periods of normal illumination. The magnitude of this effect was not anticipated, but the effect is consistent with the previous observations and the seasonal effect to be discussed.

Throughout the RPA experiment periods, corrected ML12-6 TQCM sensor temperatures remained between -32 and -37°C with the exception of one brief excursion to -38°C. Sensor temperature is important not only because it affects the re-evaporation rate of adsorbed mass, but because it also affects the quartz crystal frequency in certain temperature ranges. Changes in crystal frequency are multiplied by a mass sensitivity coefficient to yield changes in adsorbed mass. However, the dependency of ML12-6 frequency on temperature between -32 and -38°C is so small that the variation of $\dot{M}_6$ with SANG cannot be attributed to changes in crystal temperature. The depressed rates of mass accumulation are, therefore, more likely to be related to shadowing of sunlight (i.e., photochemistry) than to the secondary thermal effects of shadowing.

Mass accumulation observations have been restricted to periods of normal illumination to minimize the effects of shadowing. The initial segment of this period is also excluded in order to minimize any short-term effects of the attitude maneuver. As a result, observations have been restricted to those periods where $86° < \text{SANG} < 91°$.

The second new observation concerning the effects of sunlight on ML12-6 is that the nearly 7 percent seasonal variation in solar irradiance (ref. 8) appears to modulate $\dot{M}_6$. This effect is in addition to the gradual decrease in $\dot{M}_6$ that results from the decrease in vehicle outgassing rate.

The average ML12-6 TQCM mass accumulation rates during 12 orbital periods are plotted in figure 7. It is seen that assumptions (3) and (4) set forth in the Introduction regarding constancy of mass release and adsorption characteristics are not strictly true. In particular, there has been a gradual, approximately exponential decay in mass accumulation rate versus time with a seasonal modulation superimposed on this general trend. Note that the local maximum in $\dot{M}_6$ occurs near Day 365 (31 December 1979), or approximately at Earth's perihelion, which occurs on or about Day 2003 (3 January 1980). Similarly, a local minimum in $\dot{M}_6$ occurs near Day 2185 (3 July 1980), which was near apohelion (around 6 July 1980). The values of $\dot{M}_6$ to be presented have not been normalized for the modest changes in outgassing and adsorption rates that apparently occurred over the 4- and 3-month experimental periods.

Extraneous ML12-7 Effects

Random errors that produce small uncertainties in the measurement of M_6 produce much larger uncertainties in the measurement of M_7. Furthermore, the frequency of the ML12-7 crystal was significantly affected by the variation in temperature during these experiments. (The experiments were conducted with the sensor temperature controller turned off in order to obtain minimum sensor temperatures and, therefore, maximum rates of mass adsorption.) The $\dot{M}_7$ anomally occurred during the summer RPA experiment. Because of these factors, ML12-7 data are not included in this paper.

EXPERIMENTAL RESULTS AND DISCUSSION

Data Flow and Sources of Random Error

Flight information from the P78-2 vehicle is obtained from two separate but related sources. The first is a detailed and continuous record in the form of digital data tapes, called agency tapes, which are produced for most flight days about 6 months following the date of collection. The second source of information consists of "quick-look" data obtained from the Air Force Satellite Control Facility (AFSCF), Sunnyvale AFS, California. The ML-12 portion of this data is a moderately truncated, approximately 2-min long sampling of instrument output printed about four times per day. In contrast to agency tapes, this material is normally received within a week of its collection. Personnel responsible for P78-2 operations at Mission Control Center F, AFSCF, have provided outstanding service in effectively collecting and promptly shipping ML-12 flight data. Because of this timeliness, a decision was made to utilize AFSCF printer data as source material for preliminary assessment of RPA experiment results, even though processing truncation contributes to random error in the measurement of M.

Other sources of random error include the 1-Hz resolution of the TQCM frequency counters and any variation in the period of the counter gating pulses supplied by the spacecraft. Another increase in error results from data analysis based upon the change in, rather than the absolute value of M_6 as a function of elapsed time during an experiment period. The estimated

magnitude of the random error in ΔM_6 is calculated from a model of these truncation errors to be equal to or less than ± 1.2 ng/cm^2 about 68 percent of the time, or ± 4 ng/cm^2 at all times.

Statistical Analysis of Data Scatter

The scatter of the data from the various segments that comprise the winter and summer experiments was analyzed statistically. A least squares linear regression of ΔM_6 versus elapsed time that was made of data from each experiment segment yielded a regression coefficient equal to the average mass accumulation rate during that 5-day segment ($\dot{M}_6$), a "standard error of estimate" (ref. 9) of ΔM_6 on time ($S_{\Delta m.t}$), and a standard error in the determination of $\dot{M}_6$ (S_1) for the segment. However, because some segments contained a rather small amount of data, and because the sources of random error in the measurement of M_6 are presumably uniformly present for all segments, S_1', an improved value for S_1, was obtained for each segment as follows. First, the root mean squared standard error of the estimate $\langle S_{\Delta m.t} \rangle$ was calculated by weighting the $S^2_{\Delta m.t}$ values from each segment by $(n-2)$, where n is the number of data points comprising each segment. (A value of ± 1.52 ng/cm^2 was obtained for $\langle S_{\Delta m.t} \rangle$, and it falls outside the 99.9% confidence random error values calculated from the truncation error model. Therefore, significant sources of random error other than truncation must be present.*) Finally, this weighted mean standard error of estimate was used to calculate S_1', the standard error of each regression coefficient $\dot{M}_6$, as follows:

$$S_1' = \frac{S_1}{S_{\Delta m.t}} \cdot \langle S_{\Delta m.t} \rangle = \frac{\langle S_{\Delta M.t} \rangle}{\left[\Sigma t_i^2 - (\Sigma t_i)^2/n\right]^{1/2}} \qquad (1)$$

The results of these calculations are shown in table II. At no time did S_1' exceed ± 0.34 ng/cm^2-day.

Results

The results of the RPA winter and summer experiments are tabulated in table II and plotted in figures 8 and 9. Each value of $\dot{M}_6$ reported represents the average mass accumulation rate over a 5-day period, and the error bars shown are $\pm S_1'$. In both experiments, the mass accumulation rate was smaller when RPAV was 500 V than for other values. This is consistent with the idea that reattracted positively ionized contaminants are reflected by the grid. Less easily understood are the values of $\dot{M}_6$ when RPAV was 100 V, because theory predicts $\dot{M}_6(100) < \dot{M}_6(\text{RPAV} < 100)$. One explanation is that vehicle charging might have been more prevalent than normal during these high $\dot{M}_6$ periods. It is anticipated that the eventual availability of all agency tapes for the

* Bright, P. B., private communication.

experiment periods will provide further clues to this feature of the data.

To determine the extent to which the $\dot{M}$ values were correlated with RPAV, linear regressions of $\dot{M}_6$ versus RPAV were calculated separately with data from the winter and summer experiments. In this analysis, a single linear function was fitted to all data from each experiment. As shown in figure 4, theory results in the expectation of a more complicated functional dependence of $\dot{M}$ on RPAV. However, the size of the data set in this case did not justify fitting a more complex curve to the data. The correlation coefficients associated with these linear regressions of $\dot{M}_6$ versus RPAV were also calculated. If the data are assumed to be normally distributed, levels of confidence can be assigned to the validity of the hypothesis that $\dot{M}_6$ is negatively correlated with RPAV, i.e., that contamination is enhanced by spacecraft charging. The results of these analyses are summarized in table III.

The winter experiment results provide a level of confidence of approximately 91 percent in the negative correlation of $\dot{M}_6$ with RPAV. The sensitivity of $\dot{M}_6$ to RPAV for the winter experiment is calculated to be

$$\frac{d\dot{M}_6}{dV} = \frac{-0.0028 \text{ ng/cm}^2\text{-day}}{\text{volt}} \tag{2}$$

between limits of $-100 \text{ V} < \text{RPAV} < 500 \text{ V}$.

The results from the recently concluded summer experiment are complicated by the fact that data points from three of the eight experiment segments are somewhat questionable, but no unimpeachable grounds were found for excluding them. These are the two smaller $\dot{M}_6(-100)$ values and the smaller $\dot{M}_6(100)$ value plotted in figure 9 with triangular symbols. The $\dot{M}_6(100)$ value is questionable because the M_6 versus time data from which it was derived could be better characterized by a "sawtooth" waveform than by a "ramp." Although $\dot{M}_6$ for the experiment segment as a whole is unusually low, values of $\dot{M}_6$ for the two individual sawtooth "teeth" in the segment closely approximate other summer values. One of the $\dot{M}_6(-100)$ values represents a period in which the data set is very small because of a temporary reduction in the number of data transmissions per day. The remaining $\dot{M}_6(-100)$ value is from the first summer experiment segment, which began 2 days after a TQCM temperature command was issued. Although thermal equilibration time required after such commands is usually only 1 day, it is variable and could influence the data set. Final resolution of TQCM behavior during these three periods will not be possible until appropriate agency tapes are examined.

If the questionable data points are excluded from analysis, the results of the summer experiment provide a 96 percent level of confidence in the negative correlation of $\dot{M}_6$ with RPAV. The sensitivity in this case is calculated to be

$$\frac{d\dot{M}_6}{dV} = \frac{-0.0019 \text{ ng/cm}^2\text{-day}}{\text{volt}} \tag{3}$$

between the limits of $-100\ V \leq RPAV \leq 500\ V$. If the questionable data points are included in the analysis, the sensitivity of $\dot{M}_6$ to RPAV for the summer is calculated to be

$$\frac{d\dot{M}_6}{dV} \qquad \frac{-\ 0.0009\ ng/cm^2\text{-day}}{volt} \tag{4}$$

and a 75 percent level of confidence in the negative correlation of $\dot{M}_6$ with RPAV is obtained.

These linear regressions, which have the form

$$\dot{M}_6(RPAV) = \dot{M}_6(0) + RPAV\ \frac{d\dot{M}_6}{dV} \tag{5}$$

were used to estimate the average percentage of the mass arriving at the detector that was ionized and had kinetic energy of less than 500 eV. This percentage is given by

$$\frac{\dot{M}^+}{\dot{M}^o + \dot{M}^+} = -\ \frac{500\ \ d\dot{M}_6/dV}{\dot{M}_6(0)} \times 100 \tag{6}$$

and the value ranges from 18 to 31 percent as shown in table III.

As noted in the discussion of extraneous effects, variations in solar irradiance appear to affect the rate of mass accumulation. Data obtained during the RPA experiment support the observation that the presence of sunlight enhances the accumulation of mass on a surface. Specifically, values of $\dot{M}_6$ during periods of shadowing ($91° \leq SANG \leq 94°$) are as much as 30 percent lower than those observed during nonshadowed periods ($86° \leq SANG \leq 91°$). In addition, values of $\dot{M}_6$ for periods of lesser average solar irradiance near perihelion are as much as 45 percent lower than those observed during periods near apohelion. During both the winter and summer experiments, accumulation rates for the shadowed ML12-7 TQCM have seldom exceeded 1 ng/cm^2-day, whereas the insolated ML12-6 TQCM rates have ranged from approximately 2 to 8 ng/cm^2-day. It is suspected that this phenonenon is the result of photochemical reactions at or near the adsorbing surface.

PRELIMINARY CONCLUSIONS AND IMPLICATIONS

The results of these two long-term experiments provide evidence that spacecraft frame charging significantly affects the rate of contamination of spacecraft surfaces at frame potential. This conclusion is preliminary because it rests on the assumptions set forth in the Introduction. The most important of these, which is uniformity of spacecraft charging over the two long experimental periods, can be validated when a continuous record of P78-2 frame potential is available. The data also indicate that adsorption rate can be a strong function of the average solar illumination of the adsorbing surface.

These results have several implications. Both theory and the results from the Satellite Surface Potential Monitor on P78-2 (ref. 10) demonstrate that dielectric surfaces are much more prone to charging than is the spacecraft frame. Because the exterior materials on most spacecraft are predominately dielectrics (solar cell cover glass, second surface metalized polymers, and second surface fused quartz mirrors), it is likely that high altitude vehicles are more subject to charging enhanced contamination than the approximately 25 percent enhancement measured in this experiment.

Even if the enhancement is only 25 percent, the useful period of on-orbit operation of contamination sensitive systems (such as low temperature radiators) could be extended 25 percent if effective means were employed to ameliorate this effect. Depending on the specifics of the spacecraft design and system requirements, amelioration techniques could include one or more of the following: coating the contamination sensitive dielectric with a transparent conductive film grounded to the vehicle frame, use of a lower resistivity dielectric together with a conductive adhesive mounting system, deployment of biased electrodes in the vicinity of sensitive surfaces such that the resulting electric field would deflect ionized contaminants from the sensitive surfaces, development of dielectrics with more favorable secondary electron emission characteristics to minimize charging, and active control of the spacecraft frame potential with electron emitters. Each of these techniques has disadvantages, but advantages may outweigh disadvantages in particular applications. For instance, indium oxide, the most widely considered conductive coating, is expensive and apparently contributes to the increase in solar absorptance of materials during the first few months on orbit (ref. 11). However, these costs may be acceptable because of increased system life. Furthermore, a technique may be feasible by which management of both ionized and neutral contaminants is combined. In this technique the neutrals would be ionized as they approached a sensitive surface and all low energy ions would be deflected from the surface with electric fields.

REFERENCES

1. Cauffman, D. P.: Ionization and Attraction of Neutral Molecules to a Charged Spacecraft, TR-0074 (9260-09)-1, The Aerospace Corp., August 1973.

2. Hall, D. F., et al.: Experiment to Measure Enhancement of Spacecraft Contamination by Spacecraft Charging, NASA SP-379, NTIS, 1975.

3. Hall, D. F., and Fote, A. A.: Preliminary Flight Results from P78-2 (SCATHA) Spacecraft Contamination Experiment, ESA SP-145, Proceedings of an ESA Symposium on Spacecraft Materials, October 1979.

4. Stevens, J. R., and Vampola, A. L., eds.: Description of the Space Test Program P78-2 Spacecraft and Payloads, SAMSO-TR-78-24, NTIS, 1978.

5. Purvis, C. K.: Configuration Effects on Satellite Charging Response, AIAA Paper No. 80-0040, Eighteenth Aerospace Sciences Meeting, Jan 1980.

6. Hall, D. F.: Flight Experiment to Measure Contamination Enhancement by Spacecraft Charging, Proceedings of the Society of Photo-Optical Instrumentation Engineers (SPIE), vol. 216, 1980, pp. 131-138.

7. Steen, P. G.: SCATHA Experiment Shadowing Study, SSS-R-78-3658, Systems, Science and Software, May 1978, pp. 163-166, 380-410.

8. Standard Solar Constant and Air Mass Zero Solar Spectral Irradiance Tables. ASTM Designation: ANSI/ASTM E 490-73a. Part 41 of 1978 Annual Book of ASTM Standards, 1978, pp. 672-675.

9. Hoel, P. G.: Elementary Statistics, Wiley, 1960, p. 149.

10. Mizera, P. F.: Natural and Artificial Charging: Results from the Satellite Surface Potential Monitor Flown on P78-2, AIAA Paper No. 80-0334, Eighteenth Aerospace Sciences Meeting, January 1980.

11. Hall, D. F., and Fote, A. A.: α_s/ε Measurements of Thermal Control Coatings on the P78-2 (SCATHA) Spacecraft, AIAA Paper No. 80-1530, Fifteenth Thermophysics Conference, July 1980.

TABLE I

AVERAGE SOLAR INSOLATION ON ML12-6 IN SOLAR CONSTANTS FOR VARIOUS SUN ANGLES

SANG (deg)	Radiator and Sensor Aperture	Aperture Only	Radiator only
80	0.31347	0.31347	0.31347
81	0.31438	0.31438	0.31438
82	0.31520	0.31520	0.31520
83	0.31593	0.31593	0.31593
84	0.31656	0.31656	0.31656
85	0.31709	0.31709	0.31709
86	0.31753	0.31753	0.31753
87	0.31787	0.31787	0.31787
88	0.31811	0.31811	0.31811
89	0.31788	0.31825	0.31780
90	0.31403	0.31645	0.31353
91	0.31058	0.30907	0.31089
92	0.31169	0.30819	0.31241
93	0.31410	0.31472	0.31397
94	0.31598	0.31681	0.31581
95	0.31644	0.31705	0.31631
96	0.31640	0.31656	0.31637
97	0.31592	0.31593	0.31592
98	0.31520	0.31520	0.31520
99	0.31438	0.31438	0.31438
100	0.31347	0.31347	0.31347

TABLE II
ML12-6 TQCM MASS ACCUMULATION RATES AT
VARIOUS RPA BIAS SETTINGS
(Grounded Aperture Grid Condition)

Grid Bias Level (Volts)	Accumulation Rate (ng/cm^2-day)	Statistical Standard Error (ng/cm^2-day)
	Winter Experiment	
+500	5.662	±0.265
-100	7.483	0.270
-10	6.761	0.308
+10	7.018	0.360
+100	8.069	0.337
	Summer Experiment	
-100	1.994	0.288
-100	2.088	0.346
+100	1.044	0.317
+100	3.550	0.314
+500	1.886	0.310
+500	2.172	0.327
-100	3.101	0.311
-100	3.000	0.345

TABLE III

CORRELATION OF ML12-6 TQCM MASS ACCUMULATION

RATES WITH RPA BIAS LEVELS

(Grounded Grid Configuration, $-100\ V \leq RPAV \leq 500\ V$)

Experiment Segment	Regression Coefficient (ng/cm^2-day)/volt	Correlation Coefficient (r)	Level of Confidence that $r < 0$	Average Ionized Mass (KE < 500 eV)
Winter	-0.0028	-0.721	~ 91%	19%
Summer (Abbreviated)	-0.0019	-0.828	~ 98%	31%
Summer (All Data)	-0.0009	-0.279	~ 75%	18%

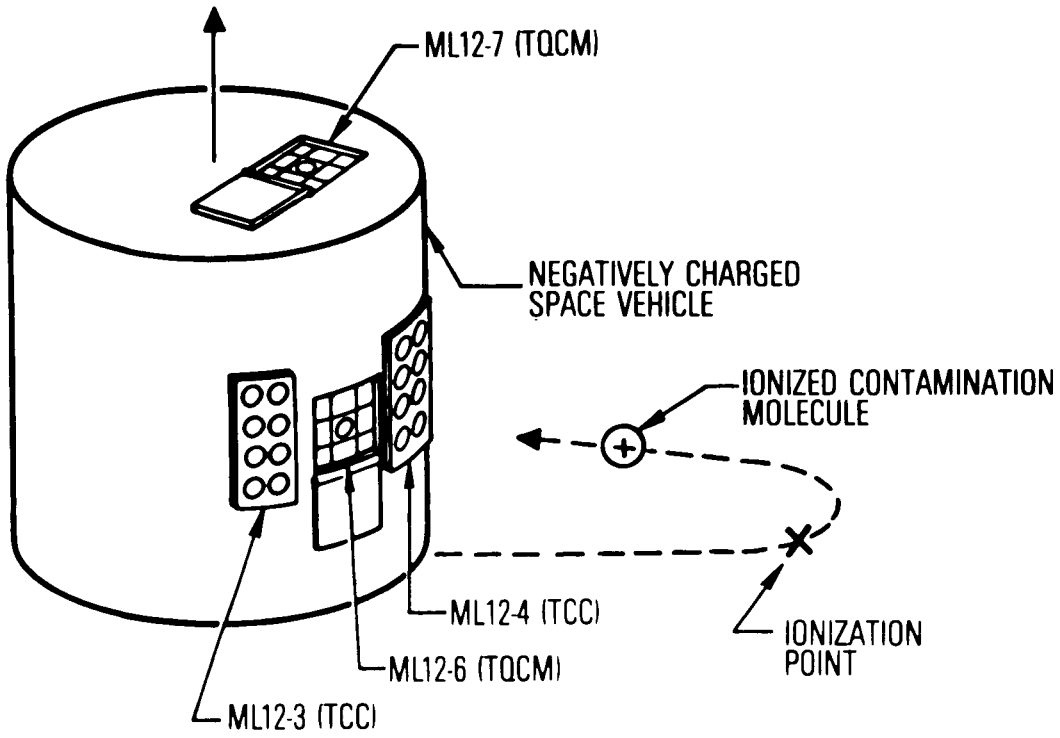

Figure 1. Placement of ML12 Sensors and Concept of Contamination Enhancement Mechanism

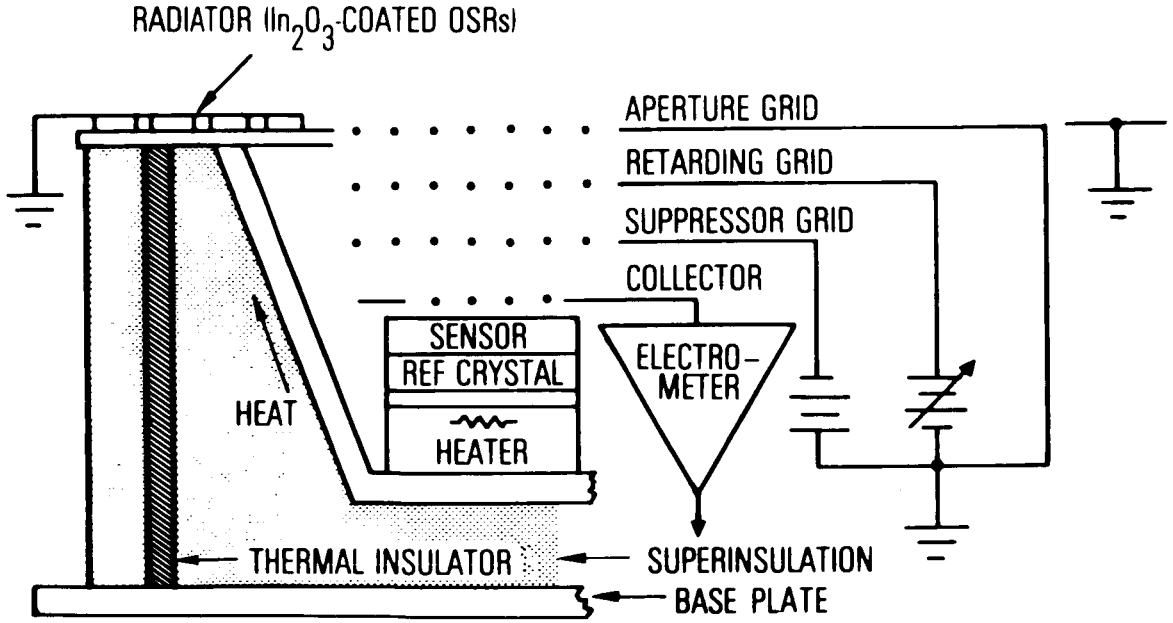

Figure 2. Schematic of RPA/TQCM sensors

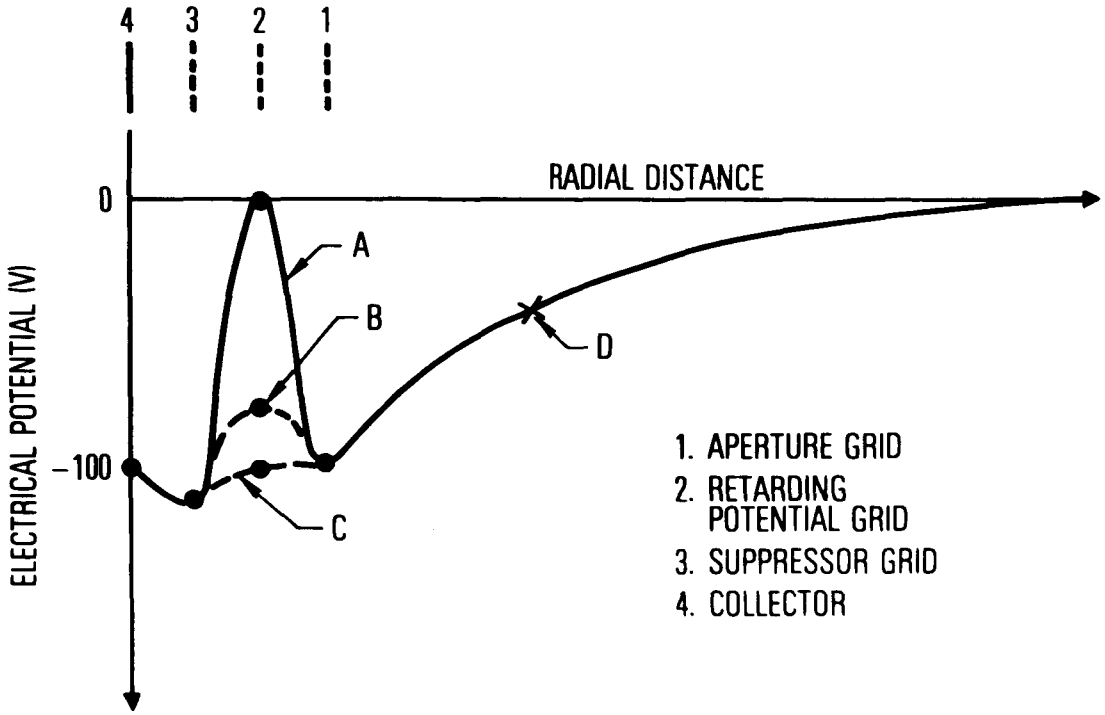

Figure 3. Potential Diagram of RPA on Negatively Charged Spacecraft Showing Three Possible Retarding Potential Grid Biases

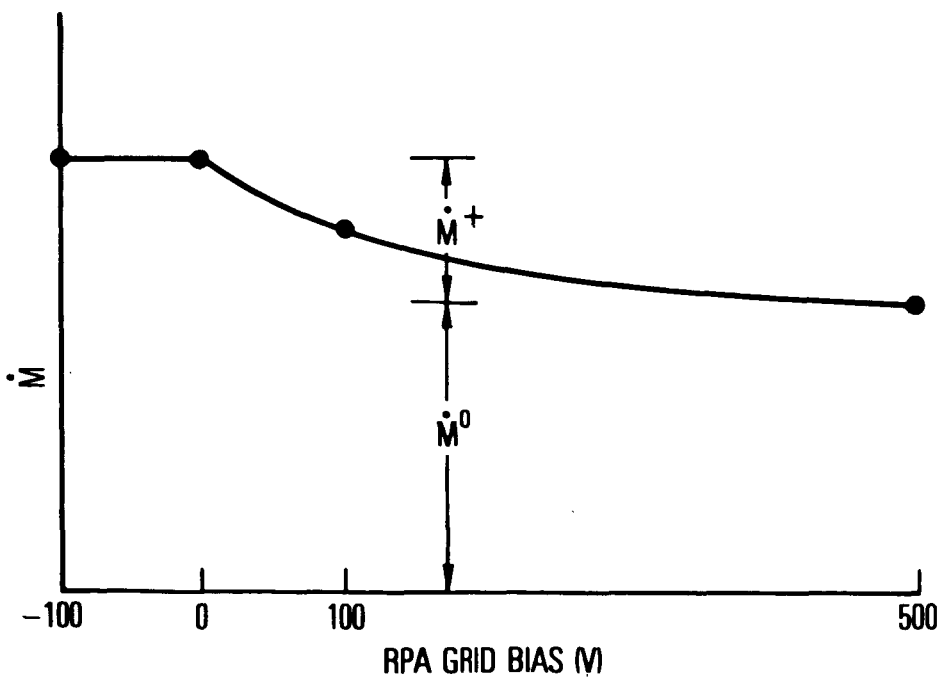

Figure 4. Theoretical Qualitative Dependence of Mass Accumulation Rate on Retarding Potential Grid Bias

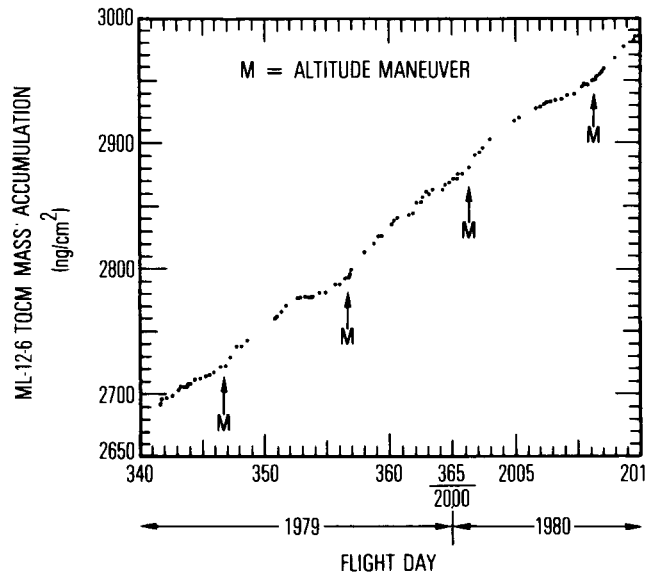

Figure 5. ML12-6 TQCM Mass Accumulation Versus Time, Expressed in Flight Days, for the Period 6 Dec. 1979 to 15 Jan. 1980

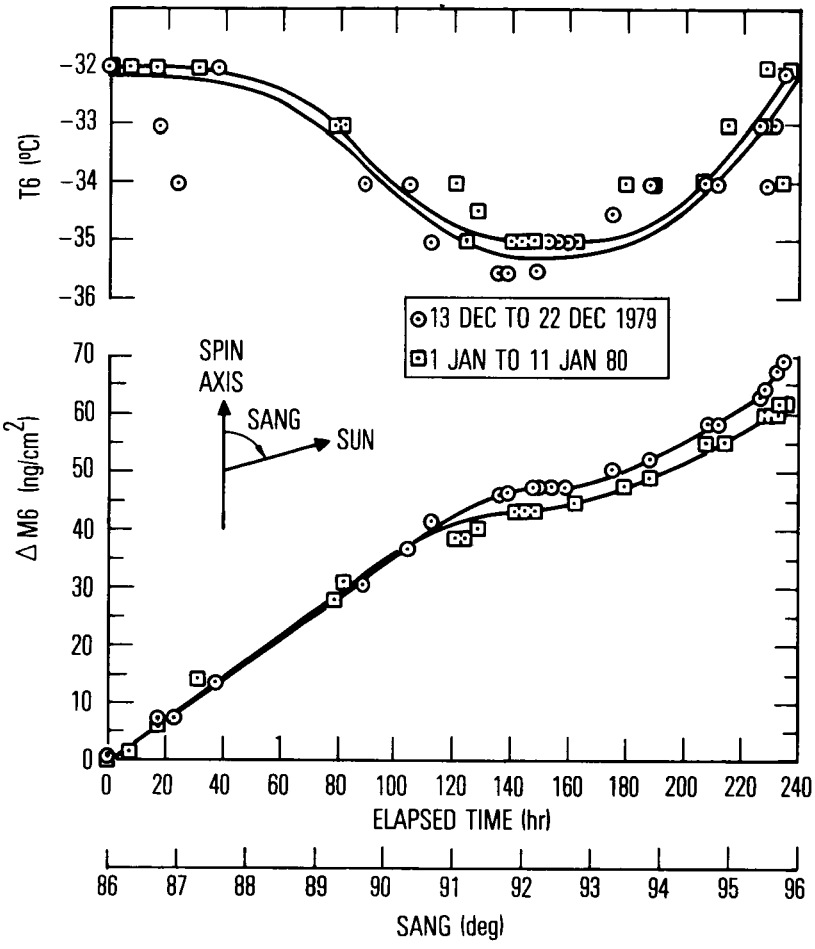

Figure 6. ML12-6 TQCM sensor Temperature (T6) and Change in Mass Accumulation (ΔM_6) Versus Elapsed Time and Vehicle Sun Angle (SANG) for the Period 13 to 22 December 1979 and 1 to 11 January 1980

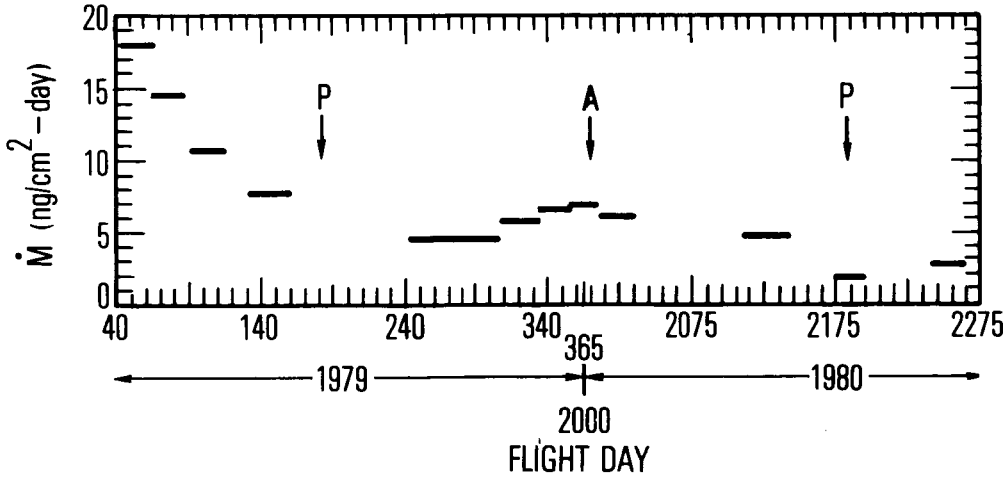

Figure 7. Equilibrium Mass Accumulation Rates of ML12-6 from Early in Flight to 1 October 1980. "P" Denotes Perihelion, "A" Denotes Apohelion

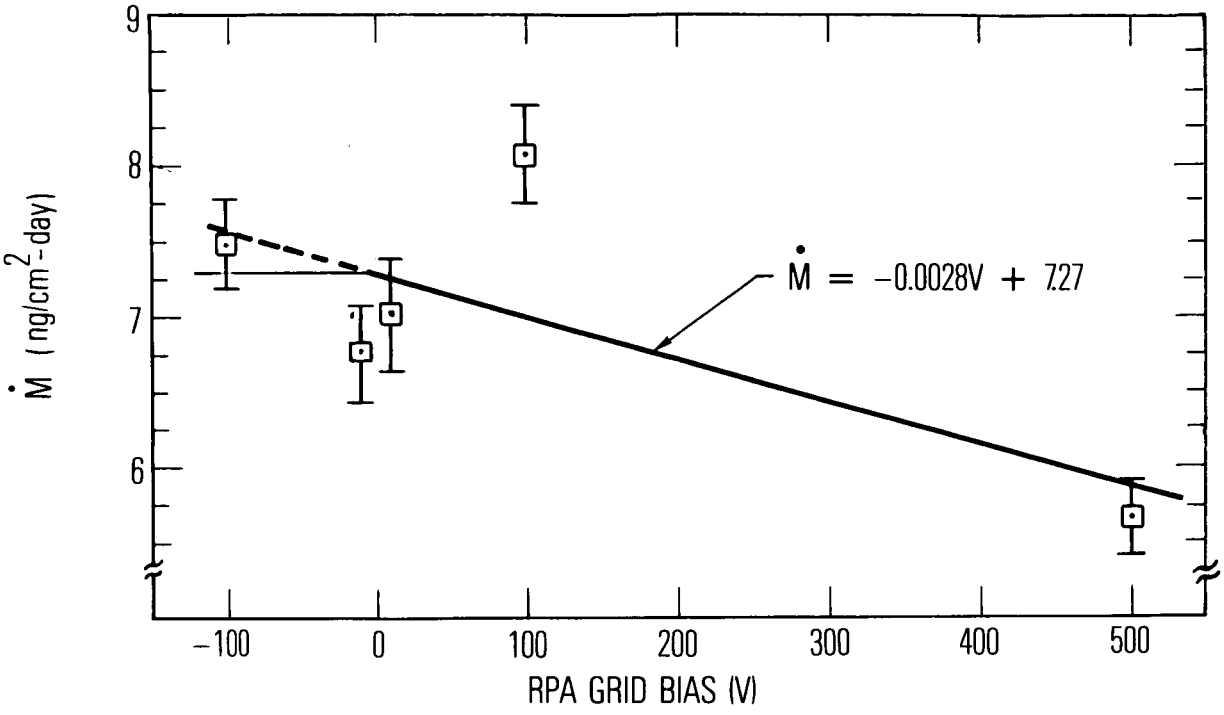

Figure 8. ML12-6 TQCM Mass Accumulation Rates at Various RPA Grid Bias Potentials During Winter Experiment

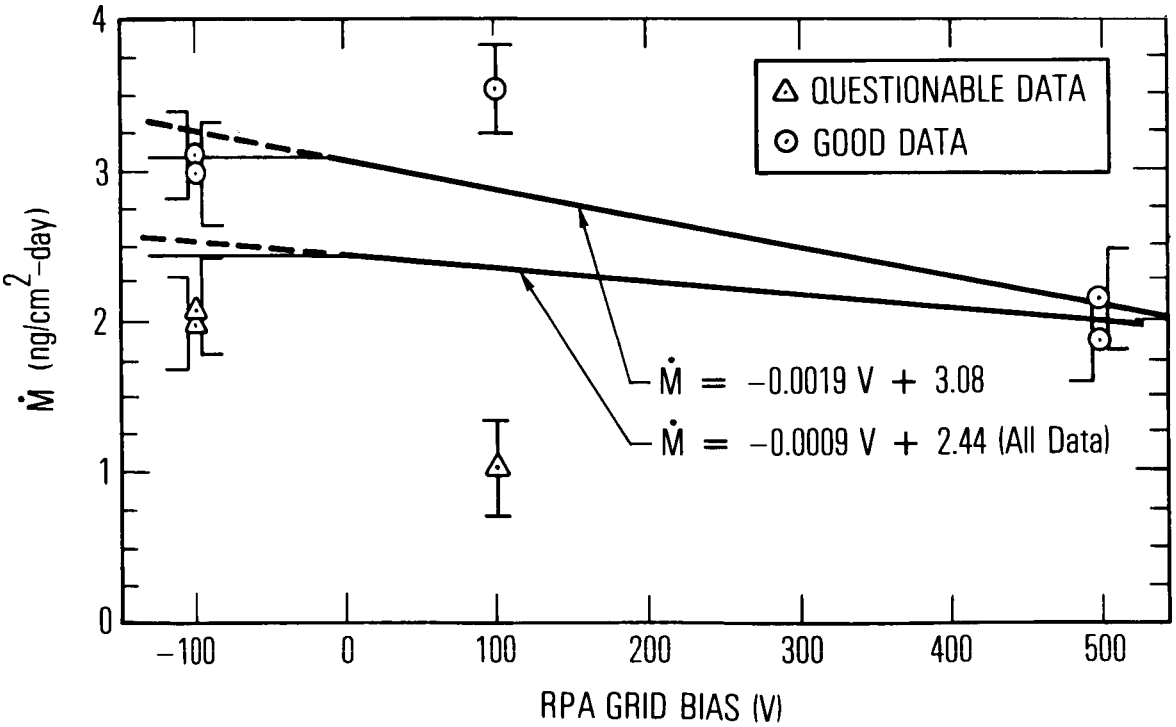

Figure 9. ML12-6 TQCM Mass Accumulation Rates at Various RPA Grid Bias Potentials During Summer Experiment